Stabilization of the Actomyosin Complex by Negative Charges on Myosin[†]

Marcus Furch,[‡] Bettina Remmel,[‡] Michael A. Geeves,[§] and Dietmar J. Manstein*,[‡]

Max-Planck-Institute for Medical Research, Department of Biophysics, Jahnstrasse 29, D-69120 Heidelberg, Germany, University of Kent, Department of Biosciences, Canterbury CT2 7NJ, Kent, U.K.

Received April 28, 2000; Revised Manuscript Received July 10, 2000

ABSTRACT: Sequence comparisons of members of the myosin superfamily show a high degree of charge conservation in a surface exposed helix (*Dictyostelium discoideum* myosin II heavy chain residues S510 to K546). Most myosins display a triplet of acidic residues at the equivalent positions to *D. discoideum* myosin II residues D530, E531, and Q532. The high degree of charge conservation suggests strong evolutionary constrain and that this region is important for myosin function. Mutations at position E531 were shown to strongly affect actin binding [Giese, K. C., and Spudich, J. A. (1997) *Biochemistry 36*, 8465−8473]. Here, we used steady-state and transient kinetics to characterize the enzymatic competence of mutant constructs E531Q and Q532E, and their properties were compared with those of a loop 2 mutant with a 20 amino acid insertion containing 12 positive charges (20/+12) [Furch et al. (1998) *Biochemistry 37*, 6317−6326], double mutant Q532E(20/+12), and the native motor domain constructs. Our results confirm that charge changes at residues 531 and 532 primarily affect actin binding with little change being communicated to the nucleotide pocket. Mutation D531Q reduces actin affinity ($\mathbf{K_A}$) 10-fold, while Q532E leads to a 5-fold increase. The observed changes in $\mathbf{K_A}$ stem almost exclusively from variations in the dissociation rate constant ($\mathbf{k_{-A}}$), with the introduction of a single negative charge at position 532 having the same effect on $\mathbf{k_{-A}}$ as the introduction of 12 positive charges in the loop 2 region.

Myosin II drives muscle contraction and motile processes such as cytokinesis and cell motility. The ATP-dependent[1] interaction of the myosin head with actin is central to myosin driven motile processes. Atomic models of the actomyosin rigor complex show the interface between myosin and actin to consist of four major contact regions, suggesting a sequential mechanism of binding (*1*, *2*). A first contact involves a highly charged, lysine-rich loop on myosin (loop 2) formed by residues S619 to V630 in the case of *Dictyostelium discoideum* myosin II and a cluster of acidic residues at the N-terminus of actin (*3*−*6*). A second contact region involves a helix-loop-helix structure formed by residues S510 to K546 (unless otherwise stated amino acid residues are numbered according to the *D. discoideum* myosin II sequence). A loop formed by residues L399 to V411 makes a third contact. These three contacts involve a single actin monomer and form the primary actin-binding site of myosin. In addition a loop protruding between residues L547 and H572 may reach the neighboring actin monomer one actin helix turn below (Figure 1).

Previously, we have shown that the light-chain-binding domain (LCBD) plays no major role in the biochemical behavior of the myosin (*7*−*9*). Recombinant constructs without LCBD can be produced and purified in large amounts and are ideally suited for systematic studies of the structure, kinetics and function of the myosin motor. Therefore, we used construct M765, corresponding to the first 765 residues of *D. discoideum* myosin II (*10*), construct M761-2R, corresponding to the first 765 residues and a C-terminal extension of two α-actinin repeats (*11*), and mutant forms of these two constructs to examine the role of a cluster of negatively charged residues in the surface exposed helix that is formed by residues S510 to K546 of the myosin heavy chain. Primary structure analysis of several myosins from various organisms suggests a high degree of functional and structural conservation in this region. Giese and Spudich (*12*) have shown that actin binding is strongly affected by mutations at position E531. Mutant E531Q was shown to greatly reduce actin-activation of myosin ATPase activity and in vitro motility. The apparent second-order rate constant for the actin-activated ATPase activity [$k_{cat}/K_{M(actin)}$] was 25-fold smaller and actin affinity in the absence of nucleotide was 10-fold lower for E531Q in comparison to the wild-type construct.

In *D. discoideum*, myosin II E531 is positioned between D530 and Q532, while in most myosins the equivalent residue is flanked by two acidic residues. Characterization of mutants E531Q and Q532E by steady-state and transient kinetics revealed that, in the absence of ATP, Q532E displays a 5-fold increase in actin-affinity over that of the wild-type

[†] Supported by the Max-Planck-Gesellschaft, Grant MA1081/5-1 by the Deutsche Forschungsgemeinschaft to D.J.M., and Grant 055841 by the Wellcome Trust to M.A.G.

* To whom correspondence should be addressed. Phone: (+49-6221) 486 212. Fax: (+49-6221) 486 437. E-mail: manstein@mpimf-heidelberg.mpg.de.

[‡] Max-Planck-Institute for Medical Research.

[§] University of Kent.

[1] Abbreviations: ADP, adenosine 5′-diphosphate; ATP, adenosine-5′-triphosphate; DEAE, diethylaminoethyl; F-actin, filamentous actin; G-actin, globular actin; mant, 2′(3′)-*O*-(*N*-methylanthraniloyl); MHF, myosin head fragment; MHC, myosin heavy chain; *mhc*A, gene encoding MHC; MOPS, 3-(*N*-morpholino)-propanesulfonic acid; n.a., not applicable; ORF, open reading frame; PCR, polymerase chain reaction; P_i, inorganic phosphate; pyr-actin, pyrene-labeled actin; S1, subfragment 1 of myosin; SDS−PAGE, sodium dodecyl sulfate−polyacrylamide gel electrophoresis.

10.1021/bi000985x CCC: $19.00
Published on Web 08/26/2000

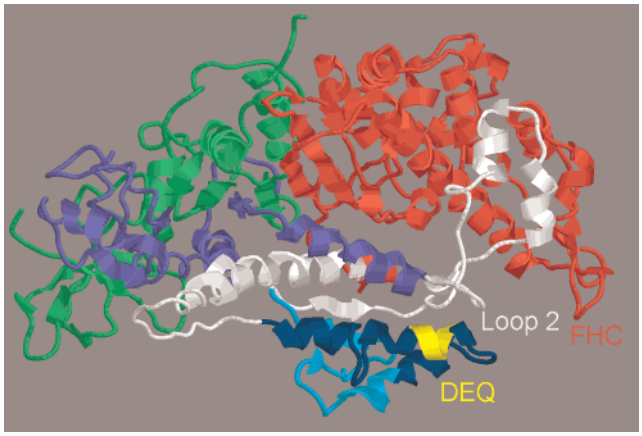

FIGURE 1: View of the actin-binding site of myosin. The ribbon diagram shows the catalytic domain of *D. discoideum* myosin II truncated after residue 754 (F. J. Kull, I. Schlichting, D. J. Manstein, and K. C. Holmes, unpublished results). The position of residues D530, E531, and Q532 is indicated in yellow. The proteolytically defined fragments are color coded as follows: N-terminal 25K, green; C-terminal 20K, violet, upper 50K, red, lower 50K, white with exception of residues 510−572. Residues S510−K546, shown in dark-blue, are forming the part of the actin binding subdomain that is involved in binding to the same actin monomer as loop 2 in the lower 50K and the familial hypertrophic cardiomyopathy loop (FHC) in the upper 50K domain. Residues L547-H572, shown in blue, form the part of the actin-binding subdomain that involves a second actin monomer. The figure was prepared by using the program RASMOL (*29*).

construct and a 50-fold increase compared to E531Q. This increase in affinity is shown to be primarily linked to slower dissociation rate constants ($\mathbf{k}_{-A}$). The presence of negative charge at position 531 or 532 leads to 14−16-fold reduction in $\mathbf{k}_{-A}$ but only a 2−3-fold decrease in the association rate constant $\mathbf{k}_{+A}$. As part of an effort to generate mutants with high actin-affinity, we additionally examined the effect of combining mutation Q532E with an increase in the number of positive charges in loop 2.

MATERIALS AND METHODS

Plasmid Construction and Mutagenesis. Molecular cloning techniques were performed as described in Sambrook et al. (*13*). Enzymes were obtained from Boehringer Mannheim and New England Biolabs. *Escherichia coli* strain XL1Blue (Stratagene, Heidelberg) was used for the amplification of plasmids. The expression vectors used for the production of mutant myosin constructs were based on pDXA-3H allowing the expression of C-terminally His_8-tagged proteins under the control of the strong constitutive *D. discoideum* actin 15 promoter (*14*).

Plasmids pDH12(E531Q)-2R and pDH12(Q532E)-2R for the production of E531Q and Q532E, respectively, were synthesized by PCR from the previously described plasmid pDH12-2R (*8*). M761-2R expressed from pDH12-2R is a fusion protein comprising the first 761 residues of the *D. discoideum- mhcA* gene linked to codon 264 extending to 505 of the *D. discoideum* α-actinin gene. Mutant constructs were generated according to the method described by Braman (*15*) using the following forward and reverse primers: 5′GTATTTTAGCTCTTTTGGATCAACAATCTGTTTTCCCAAATGCC3′ and 5′GGCATTTGGGAAAACAGATTGTTGATCCAAAAGAGCTAAAATAC3′ for E531Q; 5′GTATTTTAGCTCTTTTGGATGAAGAATCTGTTTTCCCAAATGCC3′, and 5′GGCATTTGGGAAAACAGATTCTTCATCCAAAAGAGCTAAAATAC3′ for Q532E. Nucleotide changes in the primers that lead to single amino acid substitutions are underlined. The amplified and gel-purified DNA was digested with *Eco*NI/*Bst*XI, liberating a 550-bp fragment with the mutated sequence. This fragment was subcloned into the *Eco*NI and *Bst*XI sites of pAF3-2R (*16*). A 460-bp *Bst*XI/*Bbs*I fragment from pM765(20/+12) (*10*) was inserted into the *Bst*XI/*Bbs*I sites of pDH12-(Q532E)-2R to create pM761(20/+12,Q532E)-2R. The insertion corresponds to residues 574−718 and contains 20 additional amino acids in the loop 2 region. For the production of Q532E (20/+12), which lacks the α-actinin repeat extension, a 540 bp *Eco*NI/*Bst*XI fragment was liberated from pM761(20/+12,Q532E)-2R and ligated into the *Eco*NI and *Bst*XI sites of pM765(20/+12). All DNA constructs generated for this study were confirmed by sequence analysis.

Strains and Growth Conditions. D. discoideum transformants were grown at 21 °C in HL-5C containing (per liter): 5 g of protease peptone (Merck), 5 g of Bacto yeast extract (Difco), 2.5 g of Bacto tryptone (Difco), 2.5 g of casein peptone (Merck), 10 g of D-glucose, 0.35 g of Na_2HPO_4, and 1.2 g of KH_2PO_4 (pH 6.5). Cells were either grown on 9 cm plastic Petri dishes or in 100 mL conical flasks on a gyratory shaker at 190 rpm. Plasmids were transformed into Orf^+-cells by electroporation (*17*). Transformants were selected and continuously grown in the presence of 10 μg/mL of the aminoglycoside G418 (Gibco BRL). Transformants were screened for the production of the recombinant myosin motor domains as described previously (*18*).

Protein Purification. Cells producing the wild-type and mutant myosin motor domains were grown in 5 L flasks containing 2.5 L of HL-5C. The flasks were incubated on gyratory shakers at 190 rpm and 21 °C. Cells were harvested at a density of about 5.5×10^6 mL^{-1} by centrifugation for 7 min at 2400 rpm in a Beckman J-6 centrifuge and washed once in phosphate-buffered saline. The histidine-tagged recombinant proteins were purified to homogeneity by binding to actin and release with ATP followed by Ni^{2+}-chelate affinity chromatography as described by Manstein and Hunt (*18*). An average yield of 3 mg of myosin head fragment was obtained per gram of cells. The purified proteins were >95% pure as estimated from the Coomassie blue stained SDS-polyacrylamide gel. The purified protein could be stored at −80 °C for several months without apparent loss of enzymatic activity.

Rabbit skeletal muscle actin was purified by the method of Lehrer and Kewar (*19*) with minor modifications (*10*). Actin was labeled with pyrene at Cys-374 (pyr-actin) as described (*20*). The 2′(3′)-*O*-(*N*-methylanthranilloyl) derivatives of ADP and ATP (mantADP,[1] mantATP) were prepared described by Hiratsuka (*21*). Bradford's assay was used for the determination of protein concentration (*22*).

Stopped Flow Experiments and Fluorescence Titration. Stopped-flow experiments for transient kinetics were performed at 20 °C in 20 mM MOPS, 5 mM $MgCl_2$, and 100 mM KCl, pH 7.0, with a Hi-tech Scientific SF61 or SF-61MX stopped-flow spectrophotometer (Salisbury, U.K.) using a 75 W Xe/Hg lamp and a monochromator for wavelength selection. The instrument was equipped with an automatic shutter to prevent photo bleaching during experi-

Table 1: Summary of Rate Constants for the Interaction of Nucleotides with Myosin Head Fragments[a]

nucleotide	rate constant	M765[b]	M761−2R	E531Q	Q532E	Q532E(20/+12)	(20/+12)
ATP	K_1k_{+2} ($M^{-1}s^{-1}$)	8.6×10^5	8.9×10^5	7.8×10^5	9.8×10^5	7.9×10^5	7.7×10^5
	$k_{+3}+k_{-3}$ (s^{-1})	30	30	29	29	37	36
mantATP	K_1k_{+2} ($M^{-1}s^{-1}$)	11.3×10^5	10.2×10^5	10.3×10^5	11.2×10^5	12.2×10^5	11.6×10^5
mantADP	k_{-6}/K_7 ($M^{-1}s^{-1}$)	10.2×10^5	12.1×10^5	10.0×10^5	10.1×10^5	10.2×10^5	9.9×10^5
	k_{+6} (s^{-1})	1.6	1.8	1.6	0.9	1.7	1.7
	K_D(calc) (mM)	1.6	1.5	1.6	0.9	1.7	1.7

[a] The binding and hydrolysis of ATP by *D. discoideum* myosin head fragments was analyzed in terms of the following scheme:

$$M + T \underset{k_{-1}}{\overset{k_{+1}}{\rightleftharpoons}} M{\cdot}T \underset{k_{-2}}{\overset{k_{+2}}{\rightleftharpoons}} M^{*}{\cdot}T \underset{k_{-3}}{\overset{k_{+3}}{\rightleftharpoons}} M^{**}{\cdot}D{\cdot}P_i \underset{k_{-4}}{\overset{k_{+4}}{\rightleftharpoons}} M^{*}{\cdot}D{\cdot}P_i \underset{k_{-5}}{\overset{k_{+5}}{\rightleftharpoons}} P_i + M^{*}{\cdot}D \underset{k_{-6}}{\overset{k_{+6}}{\rightleftharpoons}} M{\cdot}D \underset{k_{-7}}{\overset{k_{+7}}{\rightleftharpoons}} M + D$$

k_{+i} and k_{-i} are forward and reverse rate constants and K_i (k_{+i}/k_{-i}) is the association equilibrium constant of the ith step of the reaction. K_D corresponds to K_6K_7. Please note that in the following tables $\mathbf{K_A}$, $\mathbf{K_{AD}}$, and K_D are defined as dissociation equilibrium constants. [b] Values from Furch et al. (1998).

Table 2: Summary of Rate Constants for the Interaction of Nucleotides with Acto·M Complexes[a]

rate constant	M765[b]	M761-2R	E531Q	Q532E	Q532E(20/+12)	(20/+12)
$\mathbf{K_1k_{+2}}$ ($M^{-1}s^{-1}$)	2.5×10^5	1.4×10^5	3.3×10^5	1.3×10^5	1.2×10^5	2.1×10^5
$1/\mathbf{K_1}$ (μM)	509	360	506	284	381	403
$\mathbf{k_{+2}}$ (s^{-1})	380	626	882	503	205	339
$\mathbf{K_{AD}}$ (μM)	58	123	145	93	87	89

[a] Acto·M ATPase activity was analyzed in terms of the following scheme:

$$A{\cdot}M + ATP \overset{\mathbf{K_1}}{\rightleftharpoons} A{\cdot}M{\cdot}ATP \xrightarrow{\mathbf{k_{+2}}} A + M{\cdot}ATP \qquad A{\cdot}M{\cdot}ADP \overset{\mathbf{K_{AD}}}{\rightleftharpoons} A{\cdot}M + ADP$$

[b] Values from Furch et al. (1998) and Furch et al. (1999). $\mathbf{K_{AD}}$ is defined as dissociation equilibrium constant.

Table 3: Summary of Rate Constants for Acto·M Association and Dissociation[a]

rate constant	M765[b]	M761-2R	E531Q	Q532E	Q532E(20/+12)	(20/+12)[a]
$\mathbf{k_{+A}}$ ($M^{-1}s^{-1}$)	1.34×10^6	1.46×10^6	2.42×10^6	0.55×10^6	8.10×10^6	10.89×10^6
$\mathbf{k_{-A}}$ (s^{-1})	6.8×10^{-3}	5.2×10^{-3}	85.0×10^{-3}	0.38×10^{-3}	0.18×10^{-3}	0.44×10^{-3}
$\mathbf{K_A}$(calc) (nM)	4.5	3.6	35	0.7	0.02	0.04

[a] Actin binding was analyzed in terms of the three-state docking model:

$$A + M(\cdot N) \overset{\mathbf{K_0}}{\rightleftharpoons} \underset{\text{[collision complex]}}{A{\sim}M(\cdot N)} \overset{\mathbf{K_1}}{\rightleftharpoons} \underset{\text{[A-state]}}{A{-}M(\cdot N)} \overset{\mathbf{K_2}}{\rightleftharpoons} \underset{\text{[R-state]}}{A{\cdot}M(\cdot N)}$$

[b] Values from Furch et al. (1998). $\mathbf{k_{+A}} = \mathbf{K_0k_{+1}}$; $\mathbf{k_{-A}} = \mathbf{k_{-1}}/(1 + \mathbf{K_2})$; $\mathbf{K_A} = \mathbf{k_{-A}}/\mathbf{k_{+A}}$.

ments that were carried out on a time scale longer than 5 s. For tryptophan fluorescence, excitation was at 295 nm, with emission through a WG 320 cutoff filter (Schott, Mainz). Pyrene- and mant-fluorescence was excited at 365 nm and emission monitored after passing through a KV 389 nm cutoff filter (Schott, Mainz). Data were stored and analyzed using software provided by Hi-tech. Transients shown are the average of three to five consecutive shots of the stopped-flow machine. All concentrations refer to the concentration of the reactants after mixing in the stopped-flow observation cell. Typically working volumes of 700 μL were used to obtain one data set. The data obtained with the mutants are compared with results obtained with M761-2R or M765, which are both referred to as wild-type in this work. Unless mentioned otherwise, the experimental buffer was 20 mM MOPS, 5 mM $MgCl_2$, and 100 mM KCl, pH 7.0.

Transient Kinetic Properties of the MHF Constructs. Previous studies of M761-2R have shown that the interaction of this construct with nucleotide and actin follows the same basic mechanism that was described for S1 from rabbit fast skeletal muscle myosin and other muscle myosins (*7*, *8*). Therefore, the dynamics of ATP binding and hydrolysis by the myosin constructs were analyzed in terms of the model shown in Tables 1−3, where M refers to myosin head fragment, A to actin, and T, D, and P_i to ATP, ADP, and phosphate, respectively. In these schemes a notation is used that distinguishes between the constants in the presence and absence of actin by using bold ($\mathbf{k_{+1}}$, $\mathbf{K_1}$) versus italics type (k_{+1}, K_1); subscript A and D refer to actin ($\mathbf{K_A}$) and ADP (K_D), respectively.

The binding and hydrolysis of ATP by *D. discoideum* myosin head fragments was analyzed in terms of the seven-step model described by Bagshaw and co-workers (*23*) shown in Table 1. Transients in the presence of actin were analyzed in terms of models developed by Millar and Geeves (*24*), Geeves and Conibear (*25*), and Siemankowski and White (*26*).

Determination of ATPase Activity. Steady-state ATPase rates were measured using a linked enzyme assay as described previously (*10*). At Mg^{2+}-ATP concentrations of 0.5 mM the assays were performed in the presence of 0−80 μM actin. Estimates of the individual Michaelis−Menten parameters were obtained either directly from this presentation or from double-reciprocal plots. The values for $k_{cat}/K_{M(actin)}$ were calculated from the initial slope of the data fitted to the Michaelis−Menten equation.

RESULTS

Protein Purification. Steady-state and transient kinetics were used to analyze the effect of single point mutations

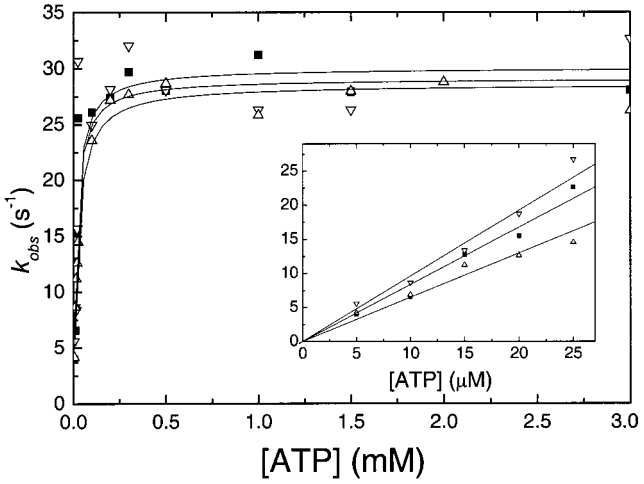

FIGURE 2: Rate of ATP-binding and ATP-hydrolysis. Myosin head fragment (0.5 μM) was mixed with an excess of ATP in a rapid mixing stopped flow fluorometer and the time dependent changes in the intrinsic protein fluorescence recorded. The fluorescence increased and could be described by an exponential function $[(F_t - F_\infty) = (F_o - F_\infty)\exp(-k_{obs}nt)]$ and k_{obs} is plotted against [ATP]. At low concentrations in the range from 0 to 25 μM the data fit a straight line (insert). The slopes of these lines define the apparent second order rate constants of ATP binding. In each case the intercept was not significantly different from zero. The symbols correspond to the following *D. discoideum* myosin constructs: M765 (■), E531Q (▽), and Q532E (△). All rate constants are summarized in Table 1. Conditions: 20 mM MOPS, 5 mM $MgCl_2$, and 100 mM KCl, pH 7.0, 20 °C.

E531Q and Q532E in the myosin motor domain on nucleotide and actin binding. Synthesis levels for both mutant constructs as well as for the parental construct M761-2R were high yielding up to 3 mg of purified protein from 1 g of cells. In contrast, mutant (20/+12)Q532E was not produced at significant levels in the M761-2R background. However, (20/+12)Q532E could be overproduced at high levels in the M765 form. Previously, we have shown that the presence of α-actinin repeats does not alter the kinetic characteristics of the motor domain (*11*). Thus we can compare the results obtained with constructs E531Q and Q532E with those obtained for Q532E (20/+12) and (20/+12) (*10*).

Interaction of Myosin Head Fragments with Nucleotides. Binding of ATP was monitored by the increase in intrinsic protein fluorescence following the addition of excess of ATP. The observed rate constants (k_{obs}) for the exponential increase in fluorescence were linearly dependent on [ATP] in the range from 5 to 25 μM (Figure 2, insert). The slope of the best-fit line defines the apparent second-order rate constant for ATP-binding (K_1k_{+2}) and the measured values were very similar for all constructs (Table 1). At higher ATP concentrations the plot of k_{obs} versus ATP concentration saturated at 0.5 mM in each case. The estimates for k_{max} were assigned to the rate of the ATP hydrolysis step ($k_{+3} + k_{-3}$), which is essentially unchanged for all the mutants yielding values between 29 and 37 s^{-1}.

Binding of mant-nucleotides to myosin head fragments was monitored by the increase in mant-fluorescence observed following addition of excess of nucleotides to each construct. For all constructs, values of 1×10^6 M^{-1} s^{-1} were obtained for the apparent second-order rate constant of both mantATP- and mantADP-binding (Table 1).

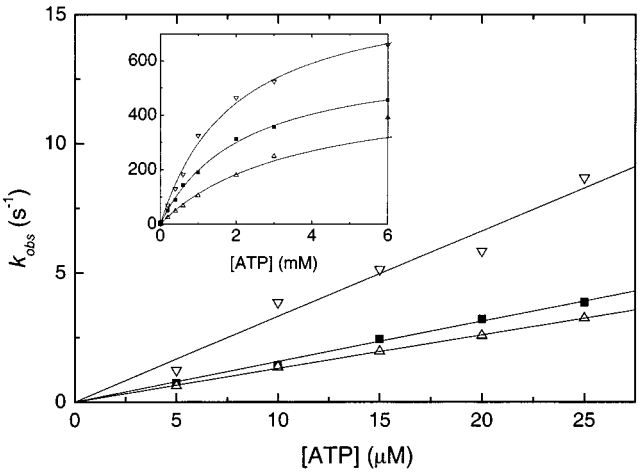

FIGURE 3: Rate of ATP induced dissociation of pyr-acto·M. At low ATP concentrations k_{obs} was linearly dependent upon [ATP] and the slopes define the second-order rate constant $\mathbf{K_1k_{+2}}$. In each case the intercept was not significantly different from zero. At higher ATP concentrations (see insert) the data could be fitted to hyperbolae as in Figure 2. The fitted parameters are listed in Table 2 where $K_{0.5}$ defines $\mathbf{K_1}$ and k_{max} defines $\mathbf{k_{+2}}$. The symbols correspond to the following *D. discoideum* myosin constructs: M765 (■), E531Q (▽), and Q532E (△). Conditions: see Figure 2.

The rate of ADP dissociation was measured by monitoring the decrease in fluorescence upon displacement of mantADP from the myosin head fragment by a large excess of ATP. The rate of mantADP release (k_{+6}) was similar for all constructs. Only Q532E gave a 2-fold lower value. The K_D for mantADP varied between 0.9 and 1.7 μM (Table 1).

ATP-Induced Dissociation of Actomyosin Motor Domain Complexes. Addition of excess ATP to pyr-actomyosin complexes results in an exponential increase in pyrene fluorescence as the actin dissociates. Values of k_{obs} were linearly dependent on [ATP] in the range from 5 to 25 μM (Figure 3). The slope of the best-fit line defines the apparent second-order rate constant $\mathbf{K_1k_{+2}}$. At higher concentrations of ATP (Figure 3, insert) the dependence of the rate constant could be fitted to a hyperbola as predicted from the scheme in Table 2. All mutant acto·M complexes display a similar ATP affinity of about 0.4 mM ATP. Values for $\mathbf{k_{+2}}$ varied between 200 and 900 s^{-1}.

ADP Inhibition of ATP-Induced Dissociation of Acto·M. The affinity of ADP for pyr-acto·M was determined from the inhibition of ATP-induced dissociation of actin from the complex. Mixing of 0.25 μM pyr-acto·M with 100 μM ATP in the presence of different amounts of ADP results in an exponential increase in fluorescence. An increase in [ADP] produced a reduction in k_{obs} for all constructs. The estimated $\mathbf{K_{AD}}$ values, obtained from the plots shown in Figure 4, ranged from 58 to 155 μM (Table 2).

Actin Binding to Myosin Head Fragments. The rate of actin binding was measured by following the exponential decrease in pyrene fluorescence observed upon adding an excess of pyr-actin to myosin head fragments. The observed rate constants were plotted against the pyr-actin concentration and in each case k_{obs} was linearly dependent upon actin concentration over the range studied (0.5−2.5 μM) (Figure 5). This is compatible with a simple one-step binding mechanism; where $k_{obs} = \mathbf{k_{+A}}[A] + \mathbf{k_{-A}}$. Thus, the apparent second-order rate constants of pyr-actin binding ($\mathbf{k_{+A}}$) are

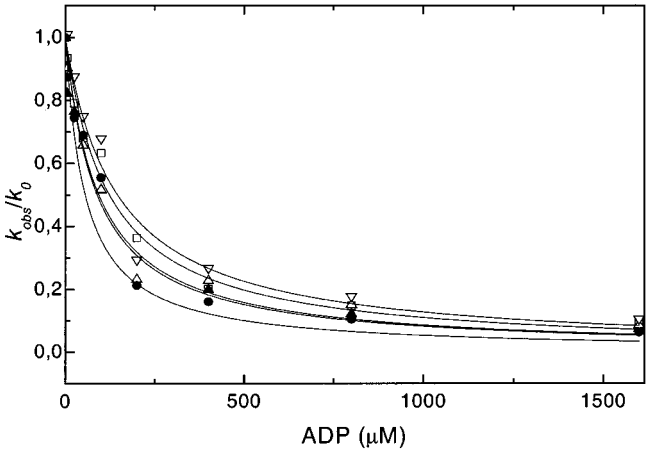

FIGURE 4: ADP inhibition of ATP-induced dissociation of pyr-acto·M. Dependence of the rate of the exponential increase in pyrene-fluorescence upon addition of 100 μM ATP to pyr-acto·M premixed with 0−1.6 mM ADP. Plot of k_{obs}/k_0 vs ADP concentration. The dissociation constants of the ADP complexes were determined by fitting a plot according to the following equation: $k_{obs}/k_0 = 1/(1 + [ADP]/\mathbf{K_{AD}})$; k_0 = observed rate constant in the absence of ADP. The values of $\mathbf{K_{AD}}$ are listed in Table 2. M765 (■), M761-2R (●), E531Q (▽), Q532E (△), and Q532E(20/+12) (▲). Conditions: see Figure 2.

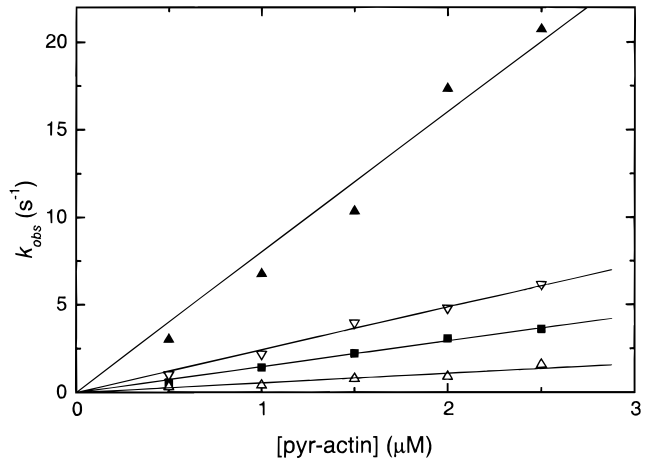

FIGURE 5: Rate of pyr-actin binding to myosin motor domain constructs. Dependence of the rate of the observed processes on pyr-actin concentration. The data were fitted to a straight line, with $\mathbf{k_{+A}}$ given by the slope. The intercepts are all near zero since the rate of dissociation is slower than the rate of association determined by these plots. M765 (■), E531Q (▽), Q532E (△), and Q532E(20/+12) (▲). Conditions were as described for Figure 2.

given by the slopes of the plots. Introduction of point mutations E531Q and Q532E had a small and opposite effect on the rate of actin binding (Table 3). Values for $\mathbf{k_{+A}}$ of 2.42×10^6 M^{-1} s^{-1} and 0.55×10^6 M^{-1} s^{-1} were obtained, respectively. Mutations Q532E(20/+12) and (20/+12) produced 6−8-fold faster actin-binding than wild-type.

The rate of actin dissociation from the myosin constructs was determined by displacing pyr-actin from pyr-acto·M with an excess of unlabeled actin (Figure 6). The observed process could be fitted to a single exponential where k_{obs} is equal to $\mathbf{k_{-A}}$. E531Q increased the rate constant for actin dissociation 16-fold, while the other mutations reduced it 10−30-fold. The ratio of the two measurements $\mathbf{k_{-A}}/\mathbf{k_{+A}}$ gives the values for the dissociation equilibrium constants for actin binding ($\mathbf{K_A}$) shown in Table 3.

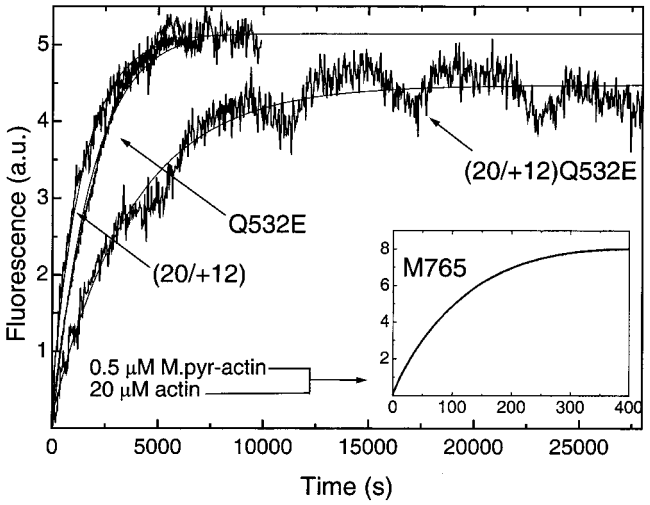

FIGURE 6: Rate of actin displacement induced by the addition of a large excess of actin to pyr-acto·M. Shown is the increase in pyrene-fluorescence during the displacement of pyr-actin from myosin head fragments (20/+12), Q523E and (20/+12)Q523E, respectively. The rate of the observed increase in fluorescence corresponds to the dissociation rate constant $\mathbf{k_{-A}}$. The insert shows the stopped flow trace for wild-type construct M765. Values for $\mathbf{k_{-A}}$ are shown in Table 3. Conditions: see Figure 2.

ATPase-Activity of Myosin Head Fragments and Acto·M. In the absence of actin, the basal Mg^{2+}-ATPase activity (k_{ATP}) of the mutant myosin constructs was similar to that of the wild-type constructs. Values varied between 0.09 s^{-1} for Q532E and 0.12 s^{-1} for Q532E(20/+12). Actin activation of ATPase activity was determined over the range from 1 to 100 μM actin. Values for k_{cat} and $K_{M(actin)}$ were estimated from a fit of the data to a hyperbolic function where possible. Where $K_{M(actin)}$ was greater than 100 μM, the values are not well-defined. However, the apparent second-order rate constant for actin binding [$k_{cat}/K_{M(actin)}$] is well-defined. Q532E has little effect on $k_{cat}/K_{M(actin)}$, whereas E531Q reduces $k_{cat}/K_{M(actin)}$ by more than 20-fold. Mutants with 12 extra charges in loop 2 have a much higher affinity for actin allowing a more accurate assessment of k_{cat} and $K_{M(actin)}$. The 20/+12 mutant has $k_{cat}/K_{M(actin)}$ increased more than 50-fold compared to wild-type, with a $K_{M(actin)}$ of 4.1 μM and a k_{cat} of 7.2 s^{-1}. The Q532E mutation in the 20/+12 background results in a ~3-fold reduction in $k_{cat}/K_{M(actin)}$ compared to 20/+12, which is due to ~2-fold decrease in k_{cat} and a ~2-fold increase in $K_{M(actin)}$ (Table 4). Compared to wild-type the changes for all constructs are dominated by changes in $K_{M(actin)}$ with small changes in k_{cat}. Thus the mutations are primarily affecting the actin-binding properties of the myosin with little change being communicated to the nucleotide pocket.

DISCUSSION

The data presented here show that the point mutations E531Q and Q532E do not affect the interaction between the myosin motor and nucleotide. The rate of ATP binding (K_1k_{+2}) and ADP binding (k_{-6}/K_7) to myosin and actomyosin ($\mathbf{K_1k_{+2}}$), the rate of ADP-dissociation from myosin (k_{+6}), and the rate of the ATP-cleavage step ($k_{+3} + k_{-3}$) remained unchanged. This suggests that the nucleotide pocket is not perturbed by the mutations. Additionally, the finding that neither the affinity of mantADP for myosin nor ADP-affinity for actomyosin was altered suggests that coupling between

Table 4: Summary of Steady-State Kinetic Parameters

	M765[a]	M761-2R	E531Q	Q532E	Q532E (20/+12)	(20/+12)[a]
basal, k_{ATP} (s^{-1})	0.08 ± 0.01	0.10 ± 0.02	0.10 ± 0.02	0.09 ± 0.02	0.12 ± 0.02	0.18 ± 0.04
k_{cat} (s^{-1})	2.8 ± 0.5	3.3 ± 0.5		4.7 ± 1.0	4.5 ± 0.5	7.2 ± 0.5
$K_{M(actin)}$ (μM)	120 ± 20	110 ± 30	>200	120 ± 30	7.2 ± 2.0	4.1 ± 0.9
$k_{cat}/K_{M(actin)}$[b] (M^{-1} s^{-1})	0.25 × 10^5	0.3 × 10^5	0.01 × 10^5	0.4 × 10^5	6.2 × 10^5	17.6 × 10^5

[a] All values from Furch et al. (1998). [b] k_{cat}/K_M(actin) was determined from the slope of the linear part of the dependence of the apparent ATPase on actin concentration. Experimental conditions: 25 mM imidazole, 25 mM KCl, 4 mM $MgCl_2$, and 6 mM ATP, pH 7.4, at 25 °C.

the nucleotide- and actin-binding sites is not perturbed by the mutations. As predicted by their location in the actin-binding site, the mutations do affect both the affinity of myosin for actin and the ability of actin to activate the myosin ATPase. The observed effects on the affinity of the constructs for actin ($\mathbf{K_A}$) stems almost exclusively from variations in the dissociation rate constant ($\mathbf{k_{-A}}$), while the changes in the association rate constant $\mathbf{k_{+A}}$ are contributing to a smaller extent. The removal of negative charge in position 531 reduces $\mathbf{K_A}$ 10-fold, while addition of negative charge in position 532 increases $\mathbf{K_A}$ 5-fold. These effects are much larger than single or double charge changes in other regions of the actin-binding site of myosin II (*9*, *10*, *27*, *28*). It is striking that the introduction of a single negative charge at position 532 has the same effect on $\mathbf{k_{-A}}$ as the introduction of 12 positive charges in the loop 2 region (see Table 2). The large effect on the dissociation rate constant is consistent with a direct contribution of the charged residue to the binding, rather than a delocalized charge effect. However, a delocalized charge effect may contribute to the smaller changes in $\mathbf{k_{+A}}$—an increase for E531Q and a decrease for Q532E—but even here the effect of a single charge change in the helix is larger than single or double charge changes in loop 2.

The opposed effects of mutations E531Q and Q532E on actin affinity can also be seen on $k_{cat}/K_{M(actin)}$. Q532E leads to a small increase in $k_{cat}/K_{M(actin)}$, while E531Q leads to a 20-fold reduction. Comparison of construct (20/+12) with the Q532E mutation in the (20/+12) background reveals a 3-fold decrease in $k_{cat}/K_{M(actin)}$ and a 2-fold increase in actin affinity ($\mathbf{K_A}$) for the double mutant. The increase in actin-affinity results mainly from a 2.5-fold slower rate of actin dissociation ($\mathbf{k_{-A}}$).

The presence of negative charge at positions 531/532 has a major affect on the actin affinity as measured by both $\mathbf{K_A}$ (primarily $\mathbf{k_{-A}}$) and $k_{cat}/K_{M(actin)}$ (primarily $K_{M(actin)}$), with little of the change in properties being communicated to the nucleotide-binding pocket. This is consistent with a two-state depiction of the myosin nucleotide pocket (strongly or weakly bound nucleotide, corresponding to the A- and R-states of the scheme in Table 3) and the charge changes at either loop 2 or at positions 531/532 only affect the concentration of actin required to induce the A to R-state structural change.

Giese and Spudich suggested that residue 531 is involved in the formation of a salt-bridge with a positively charged residue on the surface of actin, hence playing an important role in the weak to strong actin-binding transition, which is coupled to phosphate release and the power-stroke (*12*). In general, this is consistent with the data we presented here, except that we show that the primary effect is on $\mathbf{k_{-A}}$. In terms of the 3-state actin-binding model shown in Table 3, $\mathbf{k_{-A}}$ is equal to $\mathbf{k_{-1}}/(1 + \mathbf{K_2})$. The observation that coupling between actin and nucleotide binding is not influenced by either point mutation, argues against an effect on $\mathbf{K_2}$, since this is the step in which the nucleotide is effectively displaced, corresponding to the transition from the A-state with strongly bound nucleotide and weakly bound actin to the R-state with weakly bound nucleotide and strongly bound actin. Therefore, the primary effect of the mutations is probably on $\mathbf{k_{-1}}$, which controls the stability of the A-state rather than the transition to the R-state. If Giese and Spudich are correct that E531 is involved in the formation of a salt-bridge, then the 15-fold increase in $\mathbf{k_{-A}}$ is due to the loss of the salt-bridge for E531Q. In this scenario, the formation of the A-state (controlled by $\mathbf{K_0k_{+1}}$) is unaffected by the absence of the salt-bridge but the stability of the A-state is reduced due to an increase in $\mathbf{k_{-1}}$ As the equilibrium constant $\mathbf{K_0K_1}$ (=[A-state]/[A]·[M]) is sensitive to changes in $\mathbf{k_{-1}}$, the loss of the salt-bridge results in lower occupancy of the A-state at a given actin concentration and hence in a reduction in the net rate of formation of the R-state (=[A-state]·$\mathbf{k_{+2}}$). This indirect effect of the loss of charge on the rate of R-state formation can in turn be compensated by an increase in actin concentration. Thus formation of the R-state, displacement of nucleotide from the pocket, and k_{cat} appear normal at high actin concentration. This appears to be a reasonable explanation of the properties of the E531Q construct. However, if one follows this line of argument the similar reduction in $\mathbf{k_{-A}}$ observed for Q532E would require formation of a second salt-bridge. This creates a stringent restraint on any model of the actomyosin interface, which in current atomic models is not fulfilled (*1*, *2*).

The results presented here demonstrate that negatively charged residues in the region formed by residues 530−532 play a central role in defining the affinity of the myosin head for actin and in stabilizing the A-state in particular. However, the residues themselves do not play a direct role in inducing the major change in myosin, which results in displacement of the hydrolysis products and the power stroke. A more detailed interpretation of the role of these residues remains limited until we have a high-resolution structure of the actomyosin interface.

ACKNOWLEDGMENT

We thank S. Zimmermann for expert technical assistance, G. Helmig and N. Adamek for preparation of actin and pyr-actin; R. Batra for generating the expression vectors for E531Q and Q532E; M. Knetsch for discussions and providing construct M765; K.C. Holmes for continual support and encouragement.

REFERENCES

1. Rayment, I., Holden, H. M., Whittaker, M., Yohn, C. B., Lorenz, M., Holmes, K. C., and Milligan, R. A. (1993) *Science 261*, 58−65.

2. Schröder, R. R., Manstein, D. J., Jahn, W., Holden, H., Rayment, I., Holmes, K. C., and Spudich, J. A. (1993) *Nature 364*, 171−174.
3. Chaussepied, P. (1989) *Biochemistry 28*, 9123−9128.
4. Sutoh, K., Ando, M., and Toyoshima, Y. Y. (1991) *Proc. Natl. Acad. Sci. U.S.A. 88*, 7711−7714.
5. Bobkova, E. A., Bobkov, A. A., Levitsky, D. I., and Reisler, E. (1999) *Biophys. J. 76*, 1001−1007.
6. Bobkov, A. A., Bobkova, E. A., Lin, S. H., and Reisler, E. (1996) *Proc. Natl. Acad. Sci. U.S.A. 93*, 2285−2289.
7. Ritchie, M. D., Geeves, M. A., Woodward, S. K., and Manstein, D. J. (1993) *Proc. Natl. Acad. Sci. U.S.A. 90*, 8619−8623.
8. Kurzawa, S. E., Manstein, D. J., and Geeves, M. A. (1997) *Biochemistry 36*, 317−323.
9. Van Dijk, J., Furch, M., Derancourt, J., Batra, R., Knetsch, M. L., Manstein, D. J., and Chaussepied, P. (1999) *Eur. J. Biochem. 260*, 672−683.
10. Furch, M., Geeves, M. A., and Manstein, D. J. (1998) *Biochemistry 37*, 6317−6326.
11. Anson, M., Geeves, M. A., Kurzawa, S. E., and Manstein, D. J. (1996) *EMBO J. 15*, 6069−6074.
12. Giese, K. C. and Spudich, J. A. (1997) *Biochemistry 36*, 8465−8473.
13. Sambrook, J. F., Fritsch, E. F., and Maniatis, T. (1989) *Molecular cloning: a laboratory manual*, Cold Spring Harbor Laboratory Press, Plainview, NY.
14. Manstein, D. J., Schuster, H.-P., Morandini, P., and Hunt, D. M. (1995) *Gene 162*, 129−134.
15. Braman, J., Papworth, C., and Greener, A. (1996) *Methods Mol. Biol. 57*, 31−44.
16. Friedman, A. L., Geeves, M. A., Manstein, D. J., and Spudich, J. A. (1998) *Biochemistry 37*, 9679−9687.
17. Egelhoff, T. T., Titus, M. A., Manstein, D. J., Ruppel, K. M., and Spudich, J. A. (1991) *Methods Enzymol. 196*, 319−334.
18. Manstein, D. J., and Hunt, D. M. (1995) *J. Muscle Res. Cell Motil. 16*, 325−332.
19. Lehrer, S. S. and Kewar, G. (1972) *Biochemistry 11*, 1211−1217.
20. Criddle, A. H., Geeves, M. A., and Jeffries, T. (1985) *Biochem. J. 232*, 343−349.
21. Hiratsuka, T. (1983) *Biochim. Biophys. Acta 742*, 496−508.
22. Bradford, M. M. (1976) *Anal. Biochem. 72*, 248−254.
23. Bagshaw, C. R., Eccleston, J. F., Eckstein, F., Goody, R. S., Gutfreund, H., and Trentham, D. R. (1974) *Biochem. J. 141*, 351−364.
24. Millar, N. C., and Geeves, M. A. (1983) *FEBS Lett. 160*, 141−148.
25. Geeves, M. A., and Conibear, P. B. (1995) *Biophys. J. 68*, 194S-199S.
26. Siemankowski, R. F., and White, H. D. (1984) *J. Biol. Chem. 259*, 5045−5053.
27. Ponomarev, M. A., Furch, M., Levitsky, D. I., and Manstein, D. J. (2000) *Biochemistry 39*, 4527−4532.
28. Van Dijk, J., Furch, M., Lafont, C., Manstein, D. J., and Chaussepied, P. (1999) *Biochemistry* 15078−15085.
29. Sayle, R. A. and Milner-White, E. J. (1995) *Trends Biochem. Sci. 20*, 374.

BI000985X